Geomechanics and Engineering, *Vol. 17, No. 3 (2019) 237-245*
DOI: https://doi.org/10.12989/gae.2019.17.3.237

Favorable driving direction of double shield TBM in deep mixed rock strata: Numerical investigations to reduce shield entrapment

Sen Wen[1], Chunshun Zhang*[2] and Ya Zhang[1]

[1]*School of Civil Engineering and Architecture, Henan University, Kaifeng 475004, China*
[2]*Department of Civil Engineering, Monash University, Clayton, VIC 3800, Australia*

(Received July 11, 2017, Revised December 26, 2018, Accepted January 22, 2019)

Abstract. In deep mixed rock strata, a double shield TBM (DS-TBM) is easy to be entrapped by a large force during tunneling. In order to reduce the probability of the entrapment, we need to investigate a favorable driving direction, either driving with or against dip, which mainly associates with the angle between the tunneling axis and strike, θ, as well as the dip angle of rock strata, α. We, therefore, establish a 3DEC model to show the changes of displacements and contact forces in mixed rock strata through LDP (longitudinal displacement profile) and LFP (longitudinal contact force profile) curves at four characteristic points on the surrounding rock. This is followed by a series of numerical models to investigate the favorable driving direction. The computational results indicate driving with dip is the favorable tunneling direction to reduce the probability of DS-TBM entrapment, irrespective of θ and α, which is not in full agreement with the guidelines proposed in RMR. From the favorable driving direction (i.e., driving with dip), the smallest contact force is found when θ is equal to 90°. The present study is therefore beneficial for route selection and construction design in TBM tunneling.

Keywords: tunnel engineering; mixed rock strata; double shield TBM; TBM entrapment; three-dimensional numerical simulation; driving direction

1. Introduction

Tunnel boring machine (TBM) has advantages of rapid construction, safety, low noise, and vibrations so that it has been widely used in tunnel engineering throughout the world (Rostami 1997, Zhao 2007, Goh *et al.* 2018). There are many tunnels in mixed rock strata currently being excavated by TBMs, where weak and hard rocks alternately appear along the tunnel axes. This complicated rock strata condition may easily cause the TBMs to entrap, as is often reported. For instance, a TBM was jammed in different places of the Uluabat energy tunnel (Bilgin 2016) during the excavation. This is a tunnel, situated on the southern part of Uluabat Bursa (Apolyont) Lake, Turkey, where the mixed ground layer mainly consists of graphitic schist, ophiolites, melanges with boulders. Another example could be referring to Shanggongshan tunnel, a water transmission tunnel in Kunming, China; the TBM there has been entrapped for several times in mixed rock strata that comprise sandy slate and argillaceous slates, leading to a severe delay in completion of the project (Shang *et al.* 2005). Additionally, TBM entrapments also occurred during tunneling in Tao River Water Diversion Project in Gansu Province of China, resulting in at least one and a half years' delay in completion of the excavation. This is again due to mixed layers of mudstone and sandy mudstone in the rock strata.

TBM entrapment usually occurs because of the interaction between the shield and the surrounding rock mass. This interaction has been studied using analytical, empirical and numerical methods in order to reduce and control the entrapment accident (Ramoni and Anagnostou 2011). Each method has its pros and cons. For example, an analytical method is widely used in the deformation analysis of tunneling due to its simplicity, such as Zhang and Zhou (2017), and Huang *et al.* (2017); however it does not provide the longitudinal distribution of ground pressure on the shield, and thus the application of this method is limited. To resolve this disadvantage, the analytical methods are sometimes combined with empirical methods, such as in Farrokh *et al.* (2006) where a convergence-confinement method was adopted to evaluate ground pressure on a shield in Ghomroud tunnel project. Later, Farrokh and Rostami (2008, 2009) analyzed the relationship between TBM operational parameters and tunneling performance based on the field data of the same Ghomroud tunnel project. Recently, Liu *et al.* (2015) investigated the mechanism of TBM entrapment by combining both analytical and empirical methods. Although an empirical method can avoid the disadvantage of an analytical method, the method is based on field data obtained in specific projects. It is also difficult to monitor the deformation of the surrounding rock in the shield area. Although a new monitoring method was recently proposed by Huang *et al.* (2018), the reliability of applying the method to practice still needs more validation.

As a comparison, a numerical simulation can not only explore the longitudinal deformation and stress distribution but also take all kinds of complex ground conditions (Xiang *et al.* 2018); therefore the numerical method is more widely

*Corresponding author, Ph.D.
E-mail: Ivan.Zhang@monash.edu

ISSN: 2005-307X (Print), 2092-6219 (Online)

used at the time being. For instance, Ramoni and Anagnostou (2010b) used a finite element method to draw dimensionless design nomograms for different types of TBMs, where the nomograms can be used to assess the feasibility of a TBM tunneling and evaluate a potential design or operational measures. Later, Ramoni and Anagnostou (2011a) investigated the interaction between an advancing shield, tunnel lining and consolidating ground in Water-Bearing Squeezing Ground. At the same year, the same two researchers (2011b) also studied the interaction between a shield, ground, and tunnel supports in a squeezing ground. In order to achieve a more accurate and practical calculation, Zhao *et al.* (2012) adopted a 3D-FEM Model to simulate the complex interaction between a rock mass, tunnel machine, its system components, and tunnel supports. Subsequently, Hasanpour (2014) adopted a 3D finite difference program to evaluate the potential of excessive ground convergence. Simulation results include longitudinal displacement profiles (LDP) and contact force profiles (LFP) on the shields, frictional forces and required thrust to move the machine and so on. Hasanpour *et al.* (2014) discussed the effects of the advance rate during excavation cycle of a shielded TBM in a squeezing ground. Hasanpour *et al.* (2015) employed FLAC^{3D} to investigate the time-dependent behavior of the ground and its impact on the loading of the shield and required thrust to move the machine forward when tunneling with a DS-TBM. In order to reduce the probability of the TBM entrapment, overboring is a common practice; therefore, Hasanpour *et al.* (2016) discussed the impact of overboring on a shield and lining; they concluded that increasing the overboring can be considered to prevent machine from jamming in squeezing ground in some cases; however, this should be carefully optimized.

A review of the above-cited references indicates that few attentions were placed on the impact of driving directions on TBM entrapments; therefore, there appear little relevant case studies and numerical analyses in the literature. However, the importance of a favorable driving direction has been emphasized in *RMR* (Rock Mass Rating) system to improve tunneling efficiency with drilling and blasting (DB) method; naturally, when tunneling in mixed rock strata using TBM, the driving direction may also play an important role, reducing the chances of entrapments. Therefore, the focus of our present paper is to investigate the impact of DS-TBM driving direction on entrapment control and find a favorable driving direction in mixed rock strata, through a set of 3D discrete element models. The primary numerical results of our study are found to be distinguished from the traditional guidelines of driving directions proposed in *RMR*.

2. Estimate of force imposed on DS-TBM

In this part, a three-dimensional modeling method of interaction between mixed rock strata and a DS-TBM is introduced. An instance is adopted to illustrate the computational method to calculate the contact force. The variations of longitudinal tendencies of radial displacement and the contact force are also investigated.

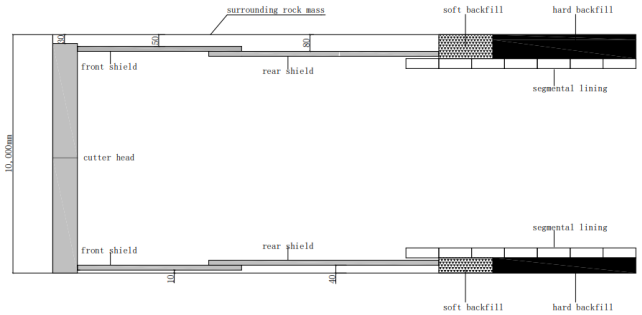

Fig. 1 Longitudinal outline of double TBM

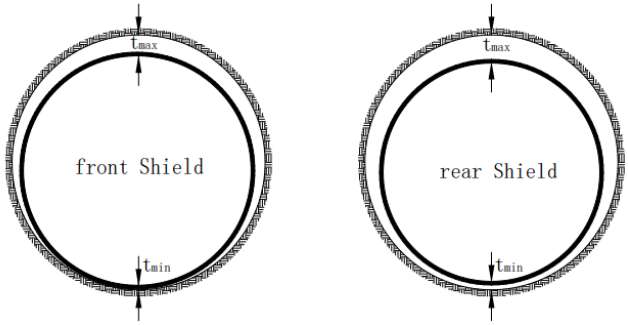

Fig. 2 Cross section of a DS-TBM at the front and the rear shields (Zhao *et al.* 2012)

2.1 Numerical modeling in 3DEC

DS-TBM allows segment installation (under the shield's protection) and driving to proceed simultaneously. Compared to a traditional DS-TBM, the more recently designed DS-TBM has a shorter shield length and stepwise reduction of the rear shield, called conicity as shown in Fig. 1 (Zhao *et al.* 2012, Hasanpour *et al.* 2014). The figure also shows the longitudinal outline of a DS-TBM and the gaps between surrounding rock and cutter head, front shield and rear shield at the crown and invert of the tunnel. As can be seen, the gaps between TBM and surrounding rock in cross section are not uniform during tunneling; the gap at the crown is considerably larger than that at the invert. Fig. 2 presents the cross sections of the DS-TBM at the front and rear shields.

The numerical model of the DS-TBM driving in the mixed rock strata is shown in Fig. 3, where Fig. 3(a) shows the whole computational model. The configurations of the cutter head, front shield, rear shield, and segmental lining are marked in different colors in Fig. 3(b). Two different types of rocks are marked in two different colors, i.e., hard rock in the dark while weak rock in the light. Fig. 3(c) shows the partially enlarged details and the layouts of the cutter head, front shield, rear shield and segmental lining (as well as soft and hard backfill materials). The thicknesses of the hard and weak rock layers are uniformly set to 2 meters. The dip angle of rock strata, α, and the angle between strike of rock strata and tunnel axis, θ, are both set to 45°. The tunnel diameter, depth and the ratio of horizontal and vertical stress are set to 10 m, 1000 m and 1, respectively. The dimension of the model is 120 × 80 × 120 m^3 (see Fig. 3). X, Y and Z coordinates denote the horizontal direction perpendicular to the tunnel axis, the

Table 1 Physical and mechanical parameters of hard, weak rock and bedding plane (Cheng *et al.* 2016)

Bedding plane			Hard and weak rock			
			Parameter	Unit	Value of hard rock	Value of weak rock
Parameter	Unit	Value	K	GPa	4.60	1.33
Normal stiffness	GPa•m^{-1}	3	G	GPa	3.31	0.80
Shear stiffness	GPa•m^{-1}	0.9	c	MPa	9	2
Friction angle	°	23	φ	°	25	24
Cohesion	MPa	1.2	ρ	kg/m^3	2780	2560
Tensile strength	MPa	0.3	σ_t	MPa	3.61	1.03

Nomenclature: K: Bulk modulus; G: Shear modulus; c: cohesion; φ: friction angle; ρ: unit weight; σ_t: tensile strength

(a) 3D computational model

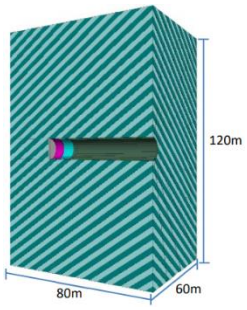

(b) Longitudinal sectional model

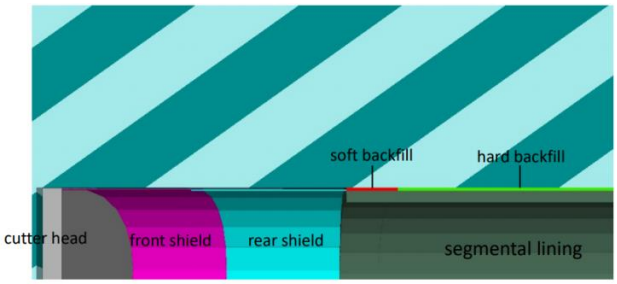

(c) Partial enlarged detail

Fig. 3 TBM construction models in 3DEC ($\theta = \alpha = 45°$)

Table 2 Mechanical and physical parameters of TBM components (Zhao *et al.* 2012, Hasanpour 2014)

Parameter	Unit	Shield	Segmental lining	Soft backfill	Hard backfill
Elastic modulus	GPa	200	36	0.5	1
Poisson's ratio	-	0.3	0.2	0.3	0.3
Unit weight	kN/m^3	76	30	24	24

direction of the tunnel axis and vertical direction, respectively. The left and right boundaries are restrained in the X direction while the front and back boundaries are fixed in the Y direction. The bottom of the model is fixed vertically, i.e., in the Z direction. Physical and mechanical parameters of mixed rock strata and mechanical parameters and geometric dimensions of TBM components are listed in Tables 1, 2 and 3, respectively. During the computation, the

Table 3 Geometric dimensions of TBM components (Zhao *et al.* 2012, Hasanpour 2014)

Parameter	Unit	Value
Cutter head length	m	0.75
Front shield length	m	5
Rear shield length	m	6
Shield thickness	cm	3
Segment width	m	2
Segment thickness	cm	45

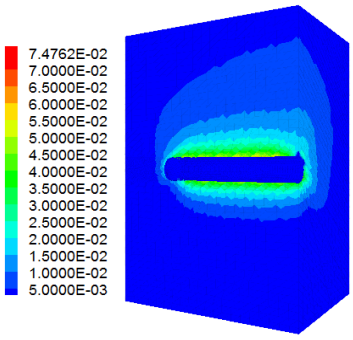

(a) Displacement contour

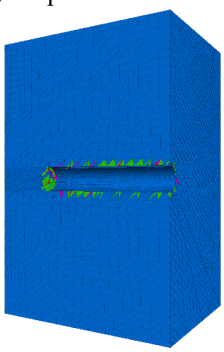

(b) Plastic zone

Fig. 4 displacement contour and plastic zone

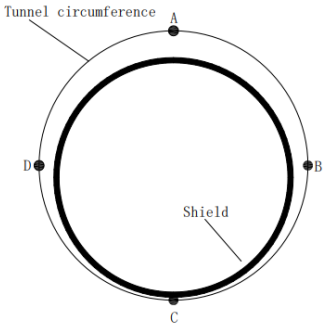

Fig. 5 Monitoring points on tunnel and shield circumference

Mohr-Coulomb criterion is used. Water pressure and consolidation problems are not taken into account in the paper.

2.2 Analysis of computational results

Whether or not the surrounding rock and shield are in

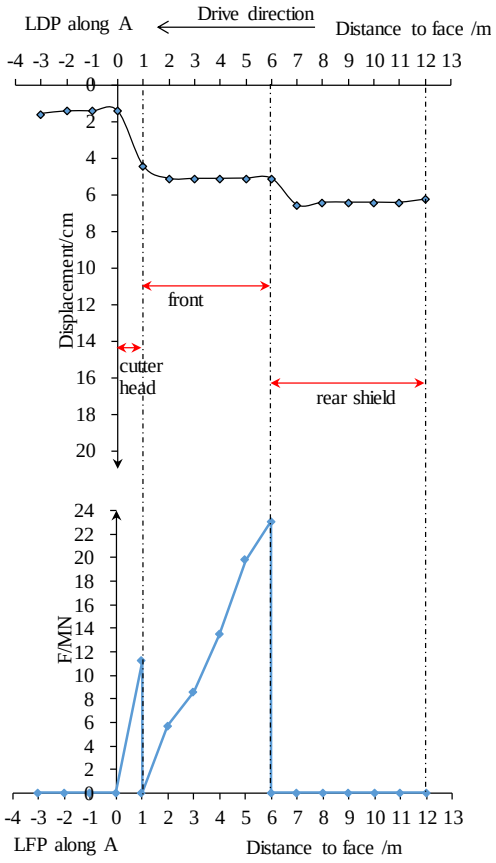

(a) LDF and LFP along A

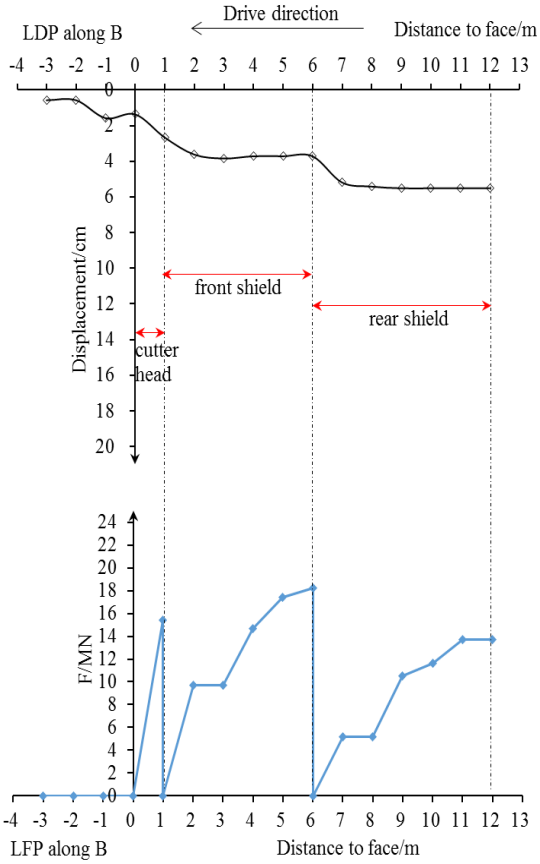

(b) LDF and LFP along B

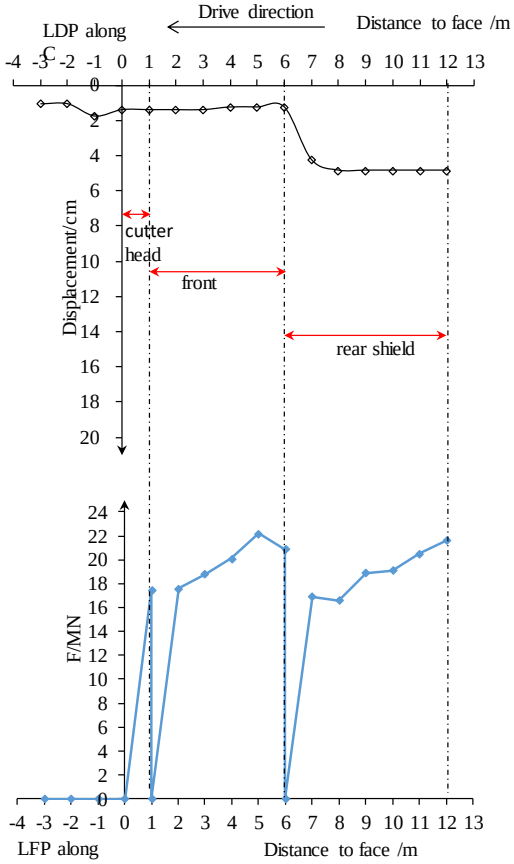

(c) LDF and LFP along C

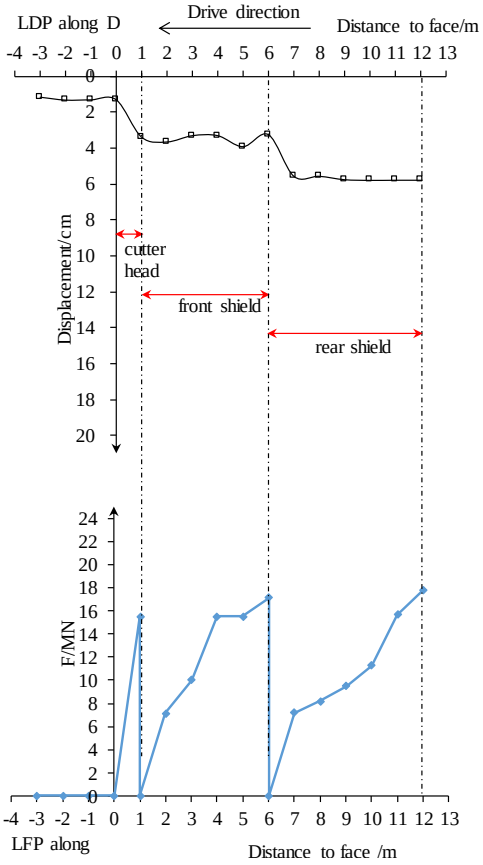

(d) LDF and LFP along D

Fig. 6 LDP and LFP

Table 4 Information of the rock strata at the four points along the tunnel axis

Point/ Distance tunnel face/m	-3	-2	-1	0	1	2	3	4	5	6	7	8	9	10	11	12
A	B	W	W	W	H	H	H	H	W	W	W	W	H	H	H	H
B	W	W	B	H	H	H	H	W	W	W	H	H	H	W	W	W
C	H	H	B	W	W	B	H	H	H	H	W	W	W	H	H	H
D	W	H	H	H	W	W	W	W	H	H	H	H	W	W	W	W

Notes : H denotes hard rock; W denotes weak rock; B denotes bedding plane between hard rock and weak rock

contact needs to be determined first before the force on the shield is calculated. Cross section is selected every one meter along the tunnel axis. In order to accurately calculate the force, every node on the tunnel circumference is assessed by Fish language program to check if it is in the contact or not. The contact fore F_i on the ith node should be calculated, which will then be used to calculate the total contact force F through Eq. (1) (Zhao 2012, Hasanpour 2014)

$$F = \sum_{i=1}^{m} F_i \tag{1}$$

where m is the maximum number of the contact points.

Fig. 4 respectively shows the displacement contour and plastic zone. Because of the confining of the shield and different gaps along the cross and longitudinal sections, more variation in the displacements at the crown along the tunnel axis can be found than that at the invert. The plastic zone is irregular because of the formation of the inclined rock strata and mainly developed along the bedding planes. Four points A, B, C and D (shown in Fig. 5) are selected as examples to further illustrate the changes of displacements and contact forces along the longitudinal direction. Their computational curves of the LDP (longitudinal displacement profile) and LFP (longitudinal contact force profile) are shown in Fig. 6.

Fig. 6 shows that the displacements (LDP) of the points A, B, C and D in front of the tunnel face (i.e., minus X coordinate) are not zero, although the local rock mass is yet to excavate. This is due to the perturbation from the previous tunneling, and the resulted displacements decrease with the increasing distance from the tunnel face.

Fig. 6 also indicates that the shield may confine the selected 4 points in driven parts by examining the values of LFP curves, i.e., the point is considered to be confined as long as its contact force F exceeds zero. As can be seen from the figure, the LDP curves of the 4 points along the longitudinal direction are almost flat, at slightly different levels depending on the locations either on the top of the front or rear shields. Through a detailed comparison, it shows the radial displacement of point A is almost the largest, irrespective of different parts of the shields. This is because the gap at the point A is the largest, compared with the gaps of other three points (as evidenced in Fig. 5), and therefore the point A could have the maximum deformation. As a result, the contact force at point A is relatively smaller, especially in the rear shield area, where the force is equal to zero while other three points have contact forces larger than zero.

Furthermore, differences of the contact forces at the regions of the cutter head, front and rear shields can be observed from Fig. 6. It is interesting to notice although the locations of the points B and D are symmetrical, the displacements and forces at both points are not the same. This could be contributed by the alternately appearing of weak and hard rocks as well as the oblique crossing between the tunnel axis and strike, such that the rock conditions at the two points are not always the same. The differences are summarized in Table 4, which also lists the information of rock strata for the other two points A and C.

3. Determination of favorable driving direction

In mixed rock strata where hard and weak rocks appear alternately, the combination of θ the angle between the tunneling axis and strike) and α (the dip angle of rock strata) plays a vital role in determining a favorable driving direction, i.e., either with or against the dip. Therefore, it requires an investigation to determine which combination should be adopted during driving to reduce the chances of TBM entrapment control.

One of the well-known guidelines was proposed by rock mass classification termed *RMR* (Rock Mass Rating) system, which evaluated the effect of the combination of α and θ. The recommendation is of *RMR* is given in Table 5 (Hoek 2006). However, note that the *RMR* system was proposed in 1976 by Bieniawski and the evaluation on the combination of α and θ mainly aimed at *DB* (drilling and blasting) method. Therefore, whether or not the evaluation can be applied to TBM should be investigated, which is our focus in the following.

We analyzed three conditions of various combinations of α and θ as follows:

1) For the tunnel axis that is parallel to the rock strike (i.e., $\theta = 0°$), any direction may achieve the same effect in reducing the entrapment.

2) For the tunnel axis that is perpendicular to the strike of rock strata (i.e., $\theta = 90°$), driving with and against dips are different in controlling the entrapment.

3) For the tunnel axis that is neither parallel nor perpendicular to the strike (i.e., $0° < \theta < 90°$), leading to an acute (driving with the dip) and obtuse (driving against the dip) angles between the driving direction and the dip, and therefore the two directions may result in different efficiency in entrapment control.

The above three conditions (i.e., $\theta = 0°$, $\theta = 90°$ and $0° < \theta < 90°$) represent typical scenarios in construction,

Table 5 Effect of discontinuity strike and dip orientation in tunneling

Strike perpendicular to tunnel axis				Strike parallel to tunnel axis		Irrespective of strike
Drive with dip		Drive against dip				
45°~90°	20°~45°	45°~90°	20°~45°	20°~45°	45°~90°	0°~20°
Very favourable	Favourable	Fair	Unfavourable	Fair	Very unfavourable	Fair

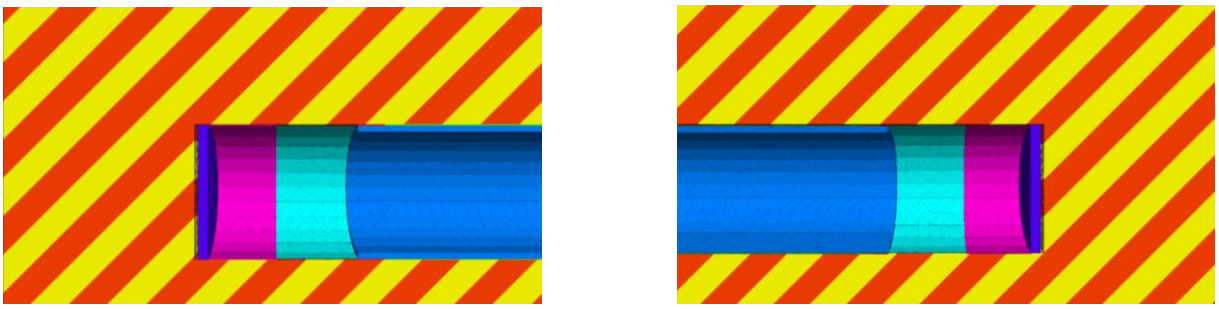

(a) Acute angle between driving direction and dip (b) Obtuse angle between driving direction and dip

Fig. 7 Longitudinal sections when tunnel axis is skew to strike of rock strata

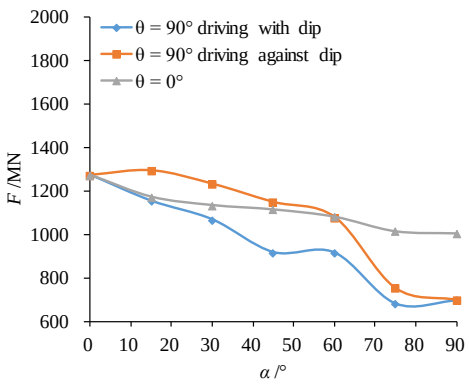

(a) Tunnel axis is perpendicular and parallel to strike

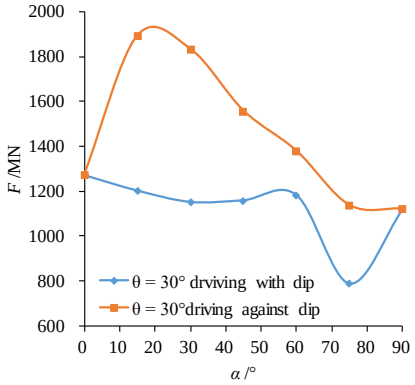

(b) The skew angle between tunnel axis and strike is 30°

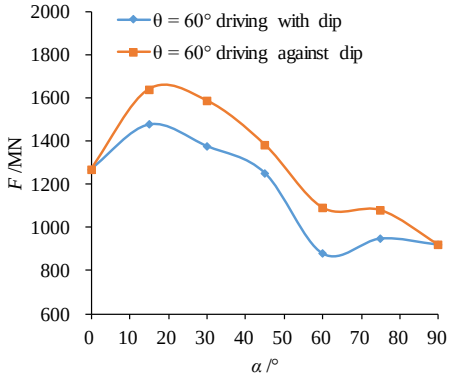

(c) The skew angle between tunnel axis and strike is 60°

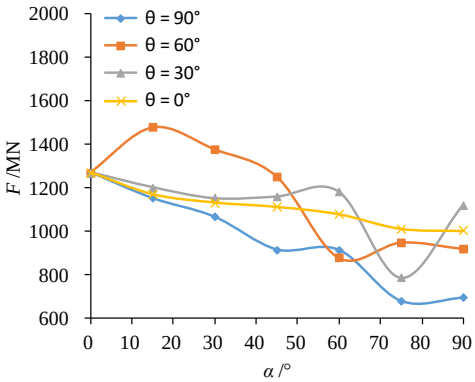

(d) Driving with dip

Fig. 8 Relationship between dip angle and total force imposed on TBM by surrounding rock

from which the favorable driving direction to minimize TBM entrapments shall be determined. This is the primary purpose of the following analysis in Section 3.1, where a series of three-dimensional discrete element models based on the model in Section 2 are carried out.

3.1 Analysis of favorable driving direction

In order to investigate the impact of different combinations of α and θ on TBM entrapments, a series of numerical calculations are conducted by 3DEC, which follows the same modeling method to that in Section 2. The parameters of the rock and TBM components are already given in Tables 1 and 2. In this section, a series of models are established from four different θ of 0°, 30°, 60°, and 90°. Also, the dip angle α for each θ is assigned to seven different values, i.e., 0°, 15°, 30°, 45°, 60°, 75°, and 90°. An example of modeling is referred to Fig.7, where shows the longitudinal sections for $0° < \theta < 90°$; in detail, Fig. 7(a) and Fig. 7(b) denote driving with and driving against dips in the same rock strata, respectively. To achieve comparable results from the both driving cases of with and against the dips, the rock stratum and all boundary conditions must remain unchanged. The TBM model in the case of driving with the dips is mirrored and placed in the same location in the case of driving against the dips. The driving direction is then assigned oppositely for each case to model the corresponding driving direction.

The computational results of the contact forces on the TBM in different dip angles are plotted in Fig. 8. When α = 0°, all the curves in Fig. 8 intersect at the same point, independent on driving directions. When α = 90°, i.e., the dip is perpendicular to tunnel axis, the contact forces resulted from driving with and against dip are the same, as

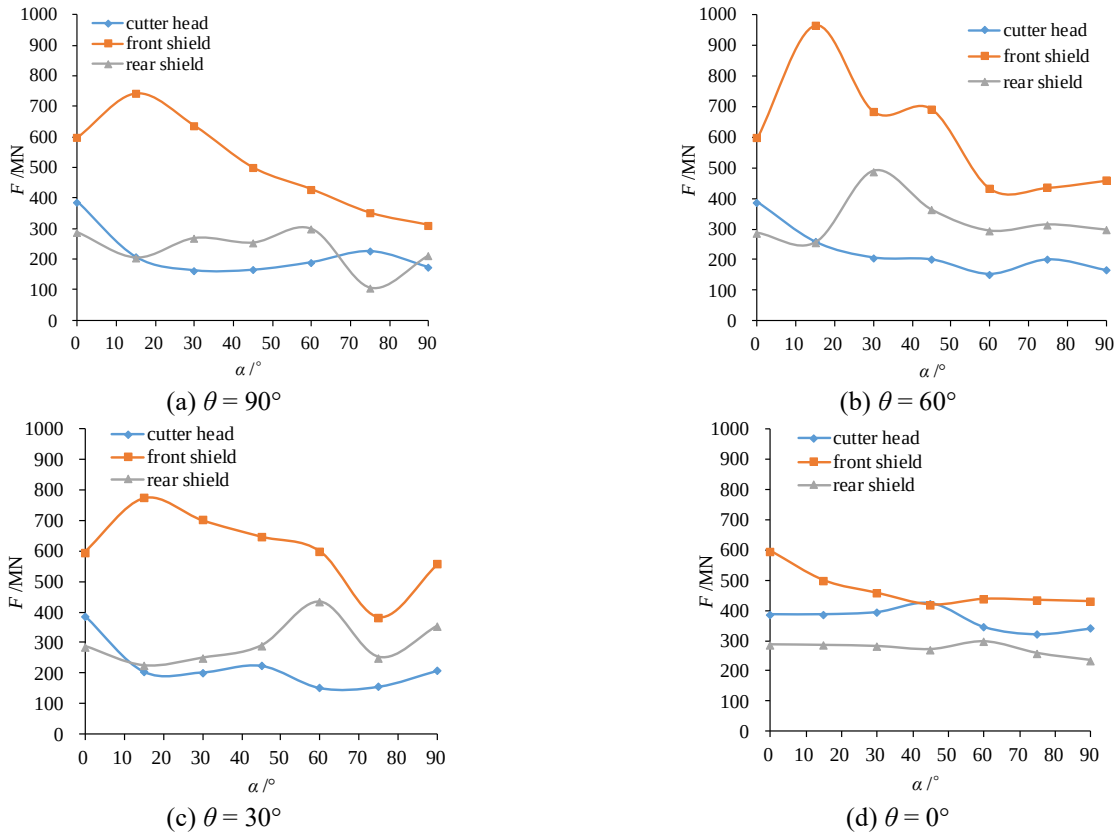

(a) $\theta = 90°$ (b) $\theta = 60°$

(c) $\theta = 30°$ (d) $\theta = 0°$

Fig. 9 Relationship between dip angle and force in different areas when driving with dip

presented in Figs. 8(a) to 8(c).

Fig. 8(a) also shows when $\theta = 0°$, with the increase of α, the contact force F gradually decreases. From $\alpha = 0°$ to 90°, F decreases by 21%, which means the increase of α can be helpful to reduce the probability of TBM entrapment. In comparison, RMR recommends that when varied from 20° to 45°, the effect on tunneling is fair, as indicated in Table 6. Additionally, *RMR* suggests that the effect on tunneling is very unfavorable when α varied from 45° to 90°, which is not in agreement with the trend shown in Fig. 8(a). Therefore, RMR guideline seems not to apply to the TBM tunneling in the direction of $\theta = 0°$.

When θ=90°, there appear two driving directions, i.e., driving with and against dips. The contact force F decreases with the increase of α in both directions, as shown in Fig. 8 (a); moreover, the contact force when driving with dip is always less than that of driving against dip, except those mentioned above two extreme values $\alpha = 0°$ and 90°. It confirms that driving with dip is better than driving against dip when $\theta = 90°$ to reduce the possibility of the TBM entrapment, which is consistent with the *RMR* guideline specified in Table 6. However, the *RMR* guideline indicates when α varies from 0° to 20°, the influence of strike of rock strata can be neglected, which is not the case for TBM. For instance, Fig. 8(a) shows that when $\alpha = 15°$, the contact force F in different θ varies significantly.

Further to explore the results of the three curves in Fig. 8(a) leads to the conclusion that the contact force induced by driving with dip is always minimum. Fig. 8(a) also shows when α = 15°,30°,45°,60° and 75°, respectively, the contact forces of driving against dip increase by 12.1%, 15.3%, 25%, 17.8%, and 10.1%, compared to the counterparts when driving with dip. Also, the same figure indicates when $\theta = 0°$, the resulted contact forces for five different α increase by 1.6%, 6.2%, 21.4%, 18%, and 48.7%, respectively, compared to those when driving with a dip at $\theta = 90°$.

Fig. 8(b) and Fig. 8(c) show the situations for $\theta = 30°$ and 60°, respectively, which show that F does not monotonically increase with increasing α, and there appear large fluctuations in the curves. Except for the two extreme dip angles (0° and 90°), F induced by driving with dip is always less than that by driving against dip, which means driving with dip is beneficial for TBM entrapment control. Comparing to driving with dip, driving against dip leads to increases of the contact forces by 57.3%, 59.0%, 34.3%, 16.5% and 44.0% as shown in Fig. 8(b), and by 10.9%, 15.1%, 10.4%, 24.2% and 13.8% as presented in Fig. 8(c).

Based on the analyses above, it can be concluded that driving with dip is always better than driving against dip irrespective of any θ. Therefore the favorable driving direction for TBM tunneling is determined, i.e., driving with dip. Under the favorable direction, we further compare the effect of θ on the contact forces, which are presented in Fig. 8 (d), where indicates that F fluctuates significantly when $\theta = 30°$ and 60°. The more regular and monotonic reduction of F with increasing α can be found for the cases of $\theta = 0°$ and 90°. Compared to all four θ cases, the lowest F is found when $\theta = 90°$, indicating the favorable angle between the tunneling axis and strike.

For TBM entrapment control, we may sum up the above findings and analyses as follows:

1) the *RMR* guideline in Table 6 is not entirely applicable to the evaluation of the favorable driving direction in TBM tunneling, and

2) the most beneficial selection is that driving with dip while $\theta = 90°$.

3.2 Comparison of contact forces in cutter head, front and rear shields

In Section 3.1, we have concluded that driving with dip is the favorable driving direction to reduce the probability of TBM entrapment. An exception is when $\theta = 0°$, any driving direction, in this case, can be considered to be favorable, as all driving directions have the same effect in controlling the entrapment. Based on the favorable driving direction, we are now looking at the changes of the contact forces on cutter head, front and rear shields in more detail in the following, as shown in Fig. 9(a) to 9(d).

The figures show the contact forces of the cutter head, front and rear shields in various dip angle α under different θ. Although the length of the rear shield is longest, its contact force is not the largest due to less influence of tunneling face, and the maximum gap between the shield and surrounding rock. As a comparison, although the length of the cutter head is far shorter (merely 0.75 m) than the front and rear shields, it is under significant contact forces close to or even larger than that of the rear shield due to the smallest gap. As for the front shield, the contact force appears to be the largest due to its length close to the rear shield while with a smaller gap. Since the front shield contributes the majority of the total contact force, the changes of both forces are quite similar. Therefore, primary attention is deserved to be paid on the performance of the front shield in entrapment control.

3.3 Discussions

The favorable driving directions discussed in the paper are based on the magnitudes of contact forces of a TBM and therefore are only applicable to the mixed rock strata that may cause TBM entrapments. In mixed rock strata where TBM is prone to be entrapped, the driving direction which is beneficial to the TBM driving cannot be entirely maintained in some cases, because of the particular geological locations of the constructions and the overall layouts of the tunneling routes. In such conditions, a proper adjustment of driving direction in some complicated local fields is suggested to reduce the probability of entrapments.

This direction adjustment can be carried out together with some other common practices to better control the entrapment, for example, through overboring (i.e., increasing the cross-section of the tunnel) to create a larger space for ground deformation, consequently reducing the forces imposed on the TBM. It is reported that a maximum overbore of 30 cm could be achieved up to date (Ramoni and Anagnostou 2010); however, too much overboring induces a more substantial plastic zone, which is harmful to the segmental lining (Hasanpour *et al.* 2016). Therefore, the determination of the amount of the overboring should not only take into account the TBM entrapment control but also consider the safety issue of the segmental lining. Another useful measure is to use a lubricant on the external surface of the shield to reduce the frictional resistance between the shield and surrounding rock mass. Besides, pre-reinforcement is another useful method; for example, foam and resin or cement admixture can be used to consolidate the fields that are likely to collapse or generate large deformations (Bayati and Hamidi 2017).

The measures mentioned above are for tunneling period. Before tunneling, there are a few other means that are worth being taken, such as using a shield with less stiffness, installing a shorter length of the shield, or adopting a cutter head in a slightly conical shape (Ramoni and Anagnostou 2010). In practical tunnel projects, there are many uncertainties about geological conditions, in-situ operations of TBM and management. To minimize the cost and delay caused by entrapments, effective means should be considered, and a prior emergency plan needs to be prepared.

4. Conclusions

For TBM entrapment control, this paper conducted a series of three-dimensional numerical simulations to investigate a favorable driving direction, which is associated with a combination of tunnel axis and strike of rock strata. In detail, the present study and obtained findings were based on the following points:

1) A 3DEC model was created to calculate the contact force imposed on a TBM. To study the profiles of displacements and contact forces around the TBM, we took four typical points as examples to show their various LDP and LFP curves, because of the different combinations of various gaps and the rock properties.

2) From the first point, a series of 3DEC models were carried out with different θ and α. Computational results demonstrate that no matter what θ and α are, driving with dip is always better than driving against dip to control entrapment; this conclusion is different from the guidelines recommended by *RMR*. In particular, irrespective of α, when θ is equal to 90° (namely the tunnel axis is perpendicular to the strike), the contact force is the smallest when driving with dip, compared with other θ.

3) The front shield is found to have the most significant contact force due to its length and distance to the rock strata, such that the shield requires the main attention in TBM entrapment control.

4) The present research findings of appropriate driving directions are obtained from estimating the magnitude of contact force on the TBM; therefore, the obtained results are only applicable to the mixed rock strata that might potentially cause TBM entrapments.

The above findings could be validated and applied to DS-TBM tunneling constructions where possible. However, this is beyond the scope of the current paper and may be studied in the future when relevant construction cases are reported.

Acknowledgements

This study was supported by the China National Natural

Science Foundation (Grant No. 51608174) and National Key Basic Research Program (973 Program) (Grant No. 2014CB046905). The first author would like to acknowledge the financial support by the China Scholarship Council.

References

Bilgin, N. (2016), "An appraisal of TBM performances in Turkey in difficult ground conditions and some recommendations", *Tunn. Undergr. Sp. Technol.*, **57**, 265-276.

Bayati, M. and Hamidi, J.K. (2017), "A case study on TBM tunnelling in fault zones and lessons learned from ground improvement", *Tunn. Undergr. Sp. Technol.*, **63**, 162-170.

Cheng J.L., Yang, S.Q., Du, L.K., Wen, S. and Zhang, J.Y. (2016), "Three-dimensional numerical simulation on interaction between double-shield TBM and surrounding rock mass in composite ground", *Chin. J. Rock Mech. Eng.*, **35**(3), 511-523.

Farrokh, E., Mortazavi, A. and Shamsi, G. (2006), "Evaluation of ground convergence and squeezing potential in the TBM driven Ghomroud Tunnel project", *Tunn. Undergr. Sp. Technol.*, **21**(5), 504-510.

Farrokh, E. and Rostami, J. (2008), "Correlation of tunnel convergence with TBM operational parameters and chip size in the Ghomroud tunnel, Iran", *Tunn. Undergr. Sp. Technol.*, **23**(6), 700-710.

Farrokh, E. and Rostami, J. (2009), "Effect of adverse geological condition on TBM operation in Ghomroud tunnel conveyance project", *Tunn. Undergr. Sp. Technol.*, **24**(4), 436-446.

Goh, A.T.C., Zhang, W.G., Zhang, Y.M., Xiao, Y. and Xiang, Y.Z. (2018), "Determination of EPB tunnel-related maximum surface settlement: A Multivariate adaptive regression splines approach", *Bull. Eng. Geol. Environ.*, **77**, 489-500

Hoek, E. (2006), Practical rock engineering, <https://www.rocscience.com/assets/resources/learning/hoek/Practical-Rock-Engineering-Full-Text.pdf>.

Hasanpour, R. (2014), "Advance numerical simulation of tunneling by using a double shield TBM", *Comput. Geotech.*, **57**, 37-52.

Hasanpour, R., Rostami, J. and Ünver, B. (2014), "3D finite difference model for simulation of double shield TBM tunnelling in squeezing grounds", *Tunn. Undergr. Sp. Technol.*, **40**, 109-126.

Hasanpour, R., Rostami, J. and Barla, G. (2015), "Impact of advance rate on entrapment risk of a double-shielded TBM in squeezing ground", *Rock Mech. Rock Eng.*, **48**(3), 1115-1130.

Hasanpour, R., Rostami J. and Özcelik Y. (2016), "Impact of overcut on interaction between shield and ground in the tunneling with a double-shield TBM", *Rock Mech. Rock Eng.*, **49**(5), 2015-2022.

Huang, X., Liu, Q.S., Peng, X.X., Lei, G.F. and Liu, H. (2017), "Mechanism and forecasting model for shield jamming during TBM tunnelling through deep soft ground", *Eur. J. Environ. Civ. Eng.*, 1-34.

Huang, X., Liu, Q.S., Liu, H., Zhang, P.L., Pan, S.L., Zhang, X.P. and Fang, J.N. (2018), "Development and in-situ application of a real-time monitoring system for the interaction between TBM and surrounding rock", *Tunn. Undergr. Sp. Technol.*, **81**, 187-208.

Liu, Q.S., Huang ,X., Liu, J P. and Pan, Y.C. (2015), "Interaction and safety control between TBM and deep mixed ground", *J. China Coal Soc.*, **40**(6), 1213-1224.

Rostami, J. (1997), "Development of a force estimation model for rock fragmentation with disc cutters through theoretical modeling and physical measurement of crushed zone pressure", Ph.D. Thesis, Colorado School of Mines, Golden, Colorado, U.S.A.

Ramoni, M. and Anagnostou, G. (2010), "Tunnel boring machines under squeezing conditions", *Tunn. Undergr. Sp. Technol.*, **25**(2), 139-157.

Ramoni, M. and Anagnostou, G. (2011), "The interaction between shield, ground and tunnel support in TBM tunneling through squeezing ground", *Rock Mech. Rock Eng.*, **44**(1), 37-61.

Ramoni, M. and Anagnostou, G. (2010), "Thrust force requirements for TBMs in squeezing ground", *Tunn. Undergr. Sp. Technol.*, **25**(4), 433-455.

Ramoni, M. and Anagnostou, G. (2011a), "The effect of consolidation on TBM shield loading in water-bearing squeezing ground", *Rock Mech. Rock Eng.*, **44**(1), 63-83.

Ramoni, M. and Anagnostou G. (2011b), "The interaction between shield, ground and tunnel support in TBM tunnelling through squeezing ground", *Rock Mech. Rock Eng.*, **44**(1), 37-61.

Shang, Y.J., Shi, Y.Y., Zeng, Q.L., Yin, J.T. and Xue, J.H. (2005), "TBM jamming and deformation in complicated geological condition and engineering measures", *Chin. J. Rock Mech. Eng.*, **24**(1), 3858-3863.

Xiang, Y.Z., Liu, H.L., Zhang, W.G., Chu, J., Zhou, D. and Xiao, Y. (2018), "Application of transparent soil model test and DEM simulation in study of tunnel failure mechanism", *Tunn. Undergr. Sp. Technol.*, **74**, 178-184

Zhao, J. (2007), "Tunnelling in rock-present technology and future challenges", *Proceedings of the World Tunnel Congress*, Prague, Czech Republic, May.

Zhao, K., Janutolo, M. and Barla, G. (2012), "A completely 3D model for the simulation of mechanized tunnel excavation", *Rock Mech. Rock Eng.*, **45**(4), 475-497.

Zhang, J.Z. and Zhou, X.P. (2017), "Time-dependent jamming mechanism for Single-Shield TBM tunneling in squeezing rock", *Tunn. Undergr. Sp. Technol.*, **69**, 209-222.

CC